Precision pointing control for SPICA: risk mitigation phase study

Shinji Mitani*[a], Yasuhiro Kawakatsu[b], Shin-ichiro Sakai[b], Naomi Murakami[a], Toshihiko Yamawaki[a], Tadahito Mizutani[a], Keiji Komatsu[b], Hirokazu Kataza[b], Keigo Enya[b], and Takao Nakagawa[b]
[a]Tsukuba Space Center, Japan Aerospace Exploration Agency, 2-1-1 Sengen, Tsukuba-shi, Ibaraki 305-8505, Japan; [b] Institute of Space and Astronautical Science, Japan Aerospace Exploration Agency, 3-1-1 Yoshinodai, Chuo-ku, Sagamihara-shi, Kanagawa 252-5210, Japan

ABSTRACT

SPICA (Space Infrared Telescope for Cosmology and Astrophysics) is an astronomical mission optimized for mid- and far-infrared astronomy with a 3-m class telescope which is cryogenically cooled to be less than 6 K. The SPICA mechanical cooling system is indispensable for the mission but, generates micro-vibrations which could affect to the pointing stability performances. Activities to be undertaken during a risk mitigation phase (RMP) include consolidation of micro-vibration control design for the satellite, as well as a number of breadboarding activities centered on technologies that are critical to the success of the mission. This paper presents the RMP activity results on the micro-vibration control design.

Keywords: SPICA, Precision pointing control, Micro-vibration control, Attitude control

1. INTRODUCTION

SPICA (Space Infrared Telescope for Cosmology and Astrophysics) is an astronomical mission optimized for mid- and far-infrared astronomy with a 3-m class telescope which is cryogenically cooled to be less than 6 K [1, 2]. Its high spatial resolution and unprecedented sensitivity in the mid- and far-infrared will enable us to address a number of key problems in present-day astronomy, ranging from the star-formation history of the universe to the formation of planets. Figure 1 shows SPICA configuration on Sun-Earth L2 orbit. SPICA is proposed as a Japanese-led mission together with extensive international collaboration. The most important international partner is ESA.

Figure 1. SPICA on orbit configuration.

*mitani.shinji@jaxa.jp; phone 81 50 3362 6942; fax 81 29 868 5969

Space Telescopes and Instrumentation 2014: Optical, Infrared, and Millimeter Wave, edited by Jacobus M. Oschmann, Jr., Mark Clampin, Giovanni G. Fazio, Howard A. MacEwen, Proc. of SPIE Vol. 9143, 914347 · © 2014 SPIE
CCC code: 0277-786X/14/$18 · doi: 10.1117/12.2055864

The SPICA adopts a new concept of cryogenic system that uses no cryogen. The elements maintained at 4.5K, including SPICA Telescope Assembly (STA), Instrument Optical Bench (IOB) and some focal plane instruments (FPI), are refrigerated by the combined action of mechanical cooling and efficient radiative cooling in the stable thermal environment at the Sun-Earth L2 [3]. The SPICA mechanical cooling system is absolutely imperative but, on the other hand, could generate micro-vibrations which affect to the pointing stability performances [4].

In the SPICA status, a Risk Mitigation Phase (RMP) has started from 2012 to 2014. Activities to be undertaken during this period include consolidation of micro-vibration control design for the satellite, as well as a number of breadboarding activities centered on technologies that are critical to the success of the SPICA mission. This paper presents the RMP activity results on the micro-vibration control design.

2. POINTING CONTROL OVERALL DESIGN

2.1 Thermal-structural restriction on SPICA

As is well known, the big appeal of SPICA mission is 3.2 m telescope and cooled down to 6K [1 - 3]. Therefore there are characteristic thermal-structural design restriction in order to achieve the pointing stability requirement. Figure 2 shows a proposed schematic and system configuration of the SPICA spacecraft. The main truss assembly is the main load and thermal path between the bus module and SPICA Telescope Assembly (STA). The baffle and the telescope shell, which are mechanically connected with the main truss assembly, surround the STA. The thermal shields, which are also connected with the main truss assembly, are placed outside of the telescope shell to keep the temperature of the telescope shell and the baffle low enough to meet the system requirement. Mechanical cooling subsystem is mounted on Bus module and connect Joule-Thomson (JT) cooler pipe to Focal Plane Instrument Assembly (FPIA) to cool down FPI's and STA.

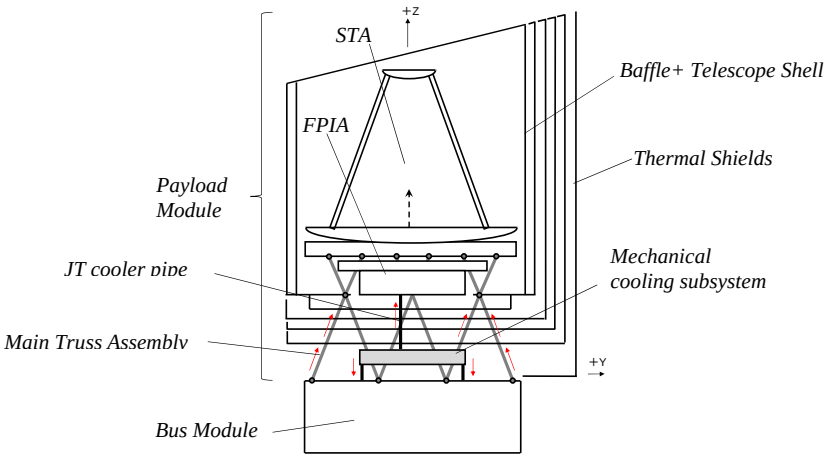

Figure 2. Schematic and system configuration of the SPICA spacecraft.

2.1.1 Mechanical cooling subsystem

The SPICA adopts a new concept of cryogenic system that uses no cryogen. The elements maintained at 4.5K, including STA, Instrument Optical Bench (IOB) and some FPIs, are refrigerated by the combined action of mechanical cooling and efficient radiative cooling in the stable thermal environment at the Sun-Earth L2. The desired temperature of 4.5 K is obtained by the JT circuit, combined with an advanced two-stage Stirling (2ST) cryocooler for precooling to 15-20 K. The increased cooling capacity of the 20 K-class 2ST cryocooler can enlarge the thermal design margin to accommodate uncertainties or incidents. There are 2 sets of 4K 2ST cryocoolers and 1K JT cryocoolers for redundancy. These total 24 units are mounted on about 1 m × 1 m square area. The cryocooler drive frequencies 15 Hz and 52 Hz about ST and JT cryocoolers respectively could be changed for the future since they are not optimized in this phase.

It should be noted that, because four JT cooler pipes are connected between FPIs and mechanical coolers, the JT pipes with ϕ 5 mm of external diameter and ~4.5 Nm^2 of equivalent flexural rigidity could leave micro-vibration transmission paths (shown in Figure 3).

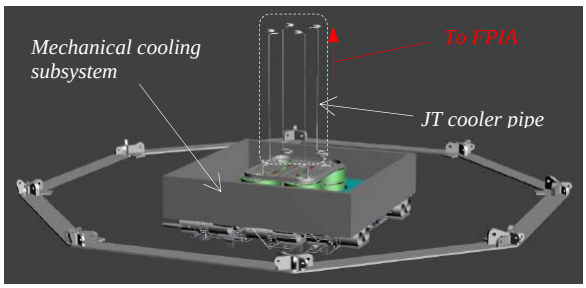

Figure 3. Mechanical cooling subsystem and JT cooler pipe.

2.1.2 Main truss assembly

A concept of the truss separation mechanisms was proposed to reduce the heat load from the bus module to the 4.5 K temperature stage in the SIA conducted by the main truss assembly in the PLM. The SPICA main truss separation mechanism is similar to the bipod and release mechanisms of GAIA [5, 6]. After the separation, the on-orbit truss which includes original octagon-shaped FRP spring only supports the STA and the IOB to prevent invasion by both heat and mechanical disturbances. Figure 4 shows the proposed separation point between middle and upper truss. The new octagon-shaped FRP springs, which are key parts of the on-orbit truss mechanism, have been manufactured in RMP. The result of the structural test are in good agreement with the design.

In addition to the motivation from the thermal design of the PLM, the truss separation mechanisms was designed for the isolation of the micro-vibration excited by the components such as mechanical cryocoolers and reaction wheels. The design of the separation mechanisms and the result of the testing with the bread-board-model are described in [7]. It was confirmed that the natural frequencies in all the 6 DOF (three in translation and three in rotation) were within the range between 1.14 and 4.84 Hz [7]. Therefore, the FRP on-orbit truss could also be effective to isolate the micro-vibration in higher frequency range (cryocooler drive frequency higher than 15 Hz) whereas structural resonance should be considered carefully.

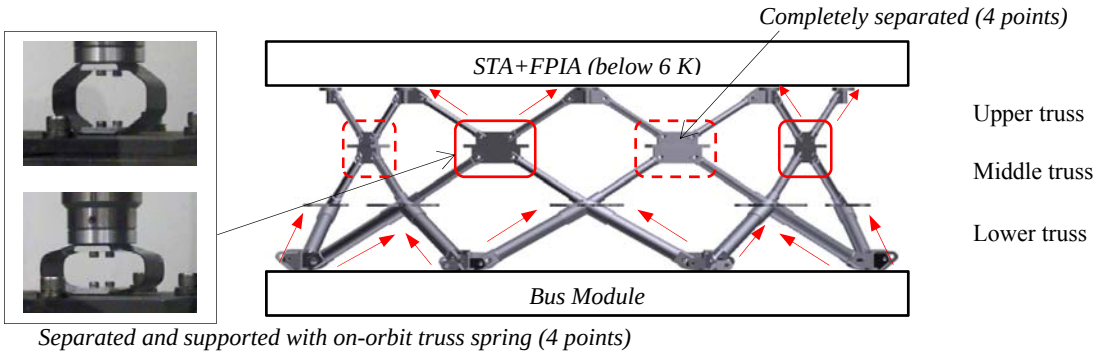

Figure 4. Truss separation mechanisms in the main truss assembly.

2.2 Precise pointing control strategy

Based on the understanding of the previous sections, we took action on the following policies in low-and high-frequency domain since the RMP. Figure 5 summarizes conceptual scheme of pointing control design and activities for risk mitigation.

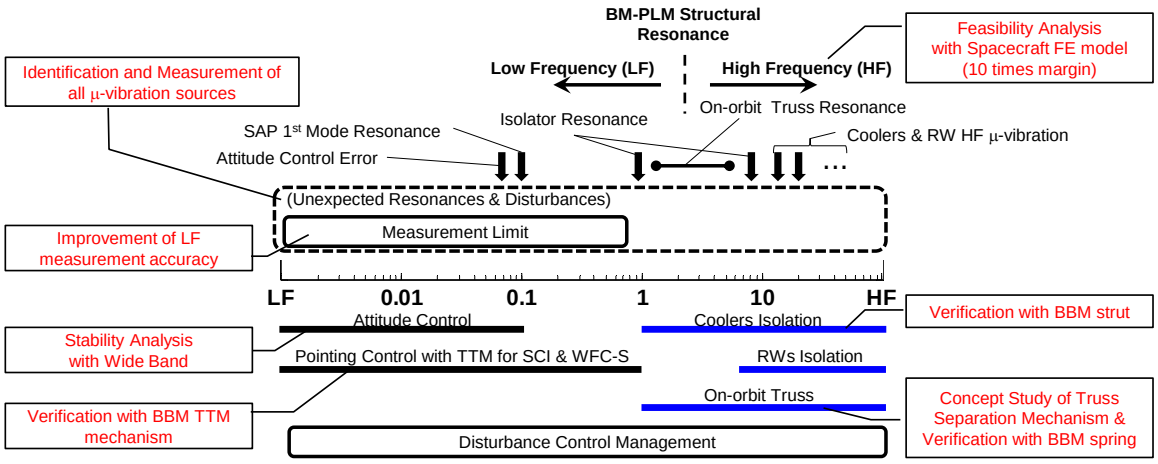

Figure 5. Conceptual scheme of pointing control design and activities for risk mitigation.

Micro vibration issue can be divided roughly in two-frequency domain by the frequency which structural resonance starts. In high-frequency domain, structural and optical resonance occurs, and estimation of FEM analysis starts to deviate from the actual measured data while critical disturbance sources exist (RW high frequency, cryocooler 15Hz, 52Hz and those harmonics). In early concept study, we concluded that installing active suppression mechanism up to several hundreds Hz is not feasible design because of heat dissipation, weight, and installing space problem etc. So isolation system in high frequency domain should be designed to ensure –40dB attenuation at 15 Hz with a only passive mechanism. In addition, on-orbit truss to isolate disturbance effectively, can also be expected. FEM analysis is conducted and pointing estimation is performed. FEM analysis are based on modal superposition method assuming Q factor of all modes are uniformly 100 (0.5% as damping). However, more conservative damping values from 0.1 % to 0.3 % are used as analysis and test in current missions [8, 9]. Therefore, high-frequency disturbance allocation is conservatively designed to ensure 10 times margin from FEM results.

In low-frequency domain, it is difficult to attenuate disturbance by passive damper because such a isolator design has too flexible stiffness. To broaden attitude control band width up to 0.1 Hz is one of the possible countermeasure plans.

In a general STT+IRU navigation, the main pointing stability error contributors in low frequency are thermo-elastic stability of the structural path between BM and PLM and the noise in the control loop comprising STT+IRU noise attenuated by a linear Kalman filtering. Therefore the FPC-G is mounted on the IOB in order to reduce significantly the alignment error between the FPI's and the FPC-G. Since the IOB is thermally stable below 6 K, it is well expected that the alignment error is less than the error budget [4].

To suppress actively pointing jitter due to micro-disturbances, Tip-Tilt Mirror (TTM) control mechanism is determined to be installed to the FPIs with stringent stability requirements : MCS-WFC and SCI to ensure the sufficient margin. The motivation of install is mainly from concealed disturbances under measurement limitation in the low frequency region. The TTM mechanism with control bandwidth up to 1 Hz and heat dissipation 1 mW at 4.5 K need to be realized.

3. MICRO-VIBRATION ANALYSIS

Detailed pointing jitter analysis were performed by SPICA Finite Elemental (FE) model. The spacecraft mass is about 3,900 kg and Principal moment of inertia are [7,800, 17,000, 17,000] kgm^2. FEM nodes have 122,295 points and free-free modes have 991 mode below 200 Hz. By superimposing all modes obtained from the FEM eigenvalue analysis, the displacement to force response functions are obtained. The damping ratio is used as 0.5 % uniform in all modes.

3.1 Mechanical cooler disturbance effect

Disturbances for all 24 sets of the mechanical coolers are measured except for 1K-JT coolers. In this phase, disturbance data of 1K-JTCL/M/H are replaced by 4K-JT data as follows:

- 1K-JTCL Replaced by 4K-JTCL
- 1K-JTCM Replaced by 4K-JTCH
- 1K-JTCH Replaced by 4K-JTCH

The disturbance is calculated at each mechanical cooler point by obtaining pointing jitter transfer functions, respectively, while the RSS contribution of the six degrees of freedom disturbance force and torque is assumed, as is the RSS contribution of each refrigerator disturbance of the same frequency. The LS contribution of the harmonics of each cooler is assumed because the phase of each of the harmonics is considered aligned. By multiplying 10 times to the value obtained in this manner, the pointing error estimation can be calculated. Figure 6 shows the pointing jitter due to mechanical cooler disturbances; separated between BOL and EOL phases.

It can be seen from the contribution of each refrigerator disturbance of each frequency band that the influence at 195 Hz is an order of magnitude higher compared with others. This is because the disturbance frequency structure resonance (13 harmonic wave of 15 Hz) point overlaps at 195 Hz.

Therefore, there is a need to contrive either to increase the stiffness of the cryocooler pedestal, or circumvent the driving frequency harmonics from the cooler pedestal resonance resonance points. The enforcement of stiffness is not readily accepted because of mass resources. Therefore the structural resonance design of the pedestal need to be carefully tuned to avoid the cryocooler harmonics in the next phase.

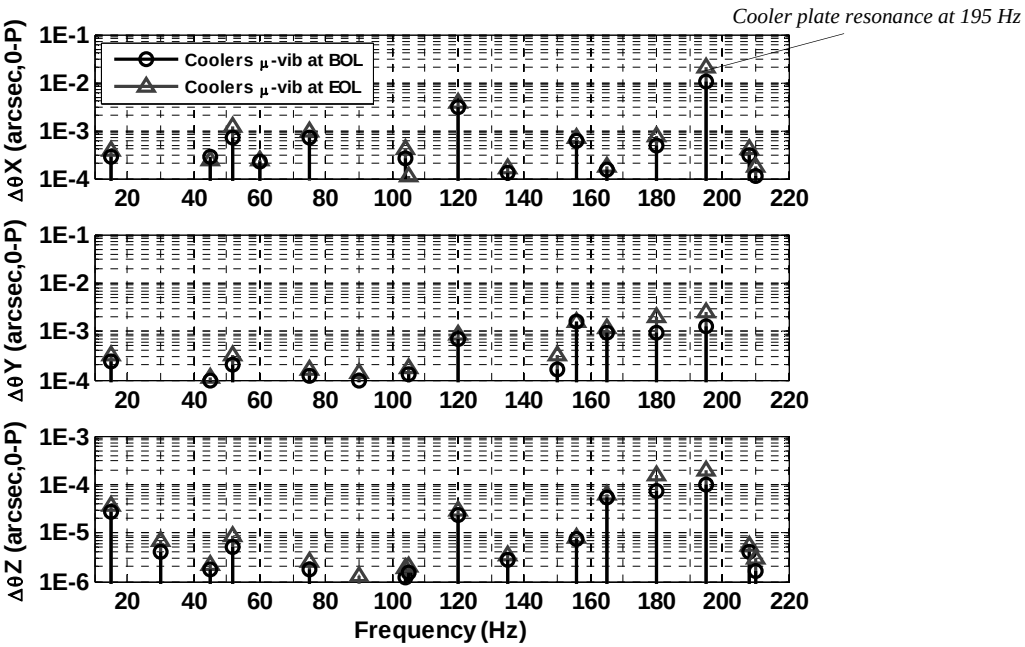

Figure 6. Power spectrum of pointing error by mechanical coolers.

3.2 Reaction wheel disturbance effect

The FEM analytical results are described, by placing the disturbance source on the RW mounting position and likewise cooler disturbances. The RW could become one of the major disturbance sources and is attachable via an isolator to the Stewart platform-type RW bracket, thus securing the capacity of the isolator mounting structure in the current model, although the isolator system is not included in the current FEM.

The single RW effect can be calculated as follows. After multiplying the change-oriented transfer function of each degree of freedom $G_{ij}(\omega)$ to the disturbance force and the torque distribution $F_d(\omega)$, $T(\omega)$ from 10 to 200 Hz, integrating 6 DOF by RSS is calculated. The pointing jitter transfer function was calculated at position points RW4. For handling the 4 RWs, it is assumed that $\sqrt{4}$ is multiplied by the result for the one RW. Attenuation 1/10 of the RW passive isolator is assumed because RW's isolation FE model is not reflected in the current version. However, this 1/10 multiplication is canceled finally since a 10-fold margin is taken. Figure 7 shows the analytical results of the 4 RWs effect on the three-axis-pointing variation. The maximum value of each axis is 10.8 mas@55.14 Hz, 15.2 mas@84.06 Hz and 0.20 mas@118.41 Hz respectively. Analysis conclusion is shown in Table 1. 15 mas (0-P) in the θ_y axis as the maximum value is excessive to 10 mas for the tentative assignment due to the high-frequency disturbance.

To meet the exact allocation, there is a need to impose a rotation operating limit on the wheel speed. It is expected that the maximum value is reduced to 2.4 mas (0-P) if limited to 2,400 RPM (40 Hz). However, the high-frequency disturbance could involve excitement, even during low-speed rotation. Therefore the limitation of the RW speed operation is to be determined in the future.

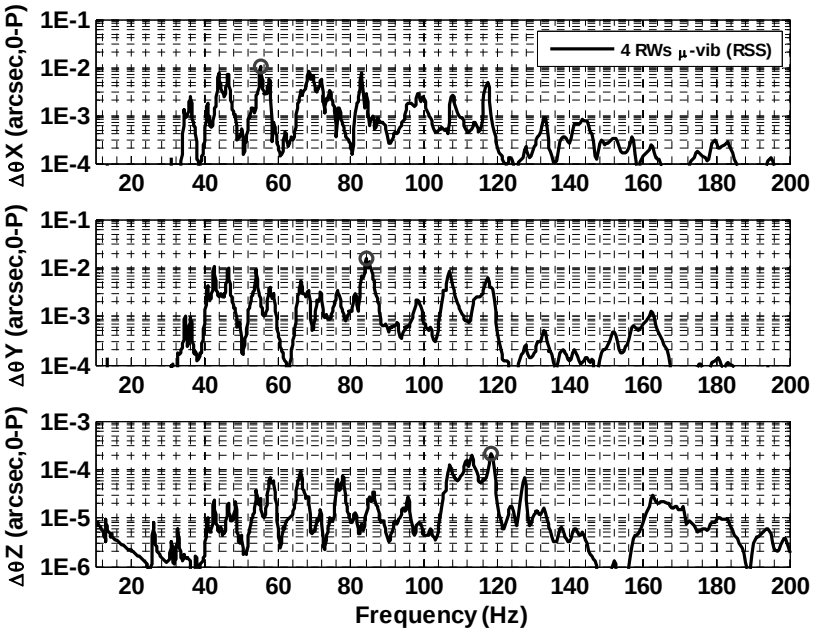

Figure 7. Power spectrum of pointing error by RWs.

Table 1. Pointing error on RW.

θ_x [mas, 0-P]	θ_y [mas, 0-P]	θ_z [mas, 0-P]	Remarks
10.8 (55.1 Hz)	15.2 (84.1 Hz)	0.20 (118.4 Hz)	with isolator, 10 margin
2.4 (36.1 Hz)	0.98 (34.6 Hz)	9.6×10^{-3} (12.9 Hz)	& Limit (Max. 2,400 RPM)
10	10	10	Allocations (tentative)

4. ISOLATOR DESIGN AND PERFORMANCE TEST

4.1 Requirement and specification

As described in the previous section, in order to satisfy the pointing stability requirements, it is necessary to reduce the disturbance level of the mechanical coolers by supporting the cooler pedestal with isolators. Table 2 shows the isolation system specification. The isolation system needs to reduce force and torque level by 1/100 at 15 Hz, which is the drive frequency of 2ST cryocooler, in all DOF. And as particular note, operational temperature is very cold and wide

(operational from –65 C to –10 C, and survival to +60 C). Due to attenuation 1/100 at 15 Hz, the strut stiffness parameters tend to be softened as needed. Due to large temperature range, needed low viscosity fluid to prevent solidification. Large temperature range (–65 C to 60 C) drives the size of the thermal chamber, since a large stroke is necessary to compensate for fluid volume change over temperature.

Therefore demonstration of the isolator is one of the key components to the feasibility of SPICA pointing stability. In RMP, the SPICA isolator was fabricated as a brassboard model. This model was designed using Honeywell D-Struts™ technology [10]. The isolator offers significant improvements over prior isolators, providing a low break frequency and featuring a tuned, three-parameter configuration that significantly outperforms the more conventional two-parameter design. A three-parameter system is one that is modeled with a spring (K_a) in parallel with a compliantly mounted damper (damper C_a in series with a spring K_b).

Table 2. Specification of isolation system on cooler pedestal.

Item	Requirement
Feature	Passive isolator, having launch lock system
Performance	Transmissibility <0.01 in all DOF @ 15 Hz, Amplification factor at resonance Q < 3
Temperature range	Operational : –65 C to –10 C (–45 C as normal) Survival : –65 C to +60 C
Size	It should be fitted to the cooler pedestal mounting portion
Weight	< 30 kg

4.2 BBM performance result

The geometry of isolation system is optimized based on mass properties from the pedestal and the strut parameters (K_a, K_b and C_a) are tuned to meet attenuation requirements on the condition that a hexapod of isolators is used (6 struts). Thermal Compensator (TC) is designed from –70 C to +60 C. Figure 8 shows fabricated SPICA isolator BBM. The functions of TC provide compliance for thermal expansion / contraction of fluid and maintain positive fluid pressure throughout the wide temperature range. The TC side mounted arrangement was used on a past flight program [11].

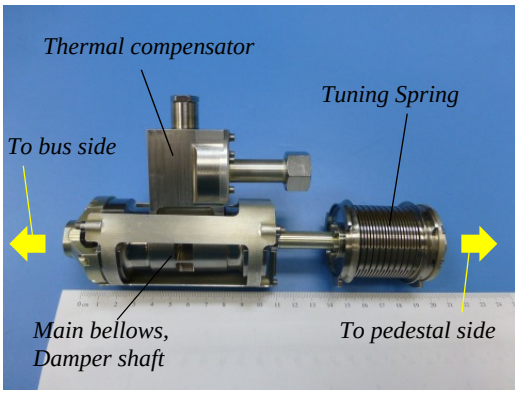

Figure 8. Picture of SPICA isolator brassboard model.

Micro-motion transmissibility test was conducted under the temperature of the isolator controlled to values at the nominal and extreme limits of the operational temperature range (–65 C to –10 C). Figure 9 shows excellent transmissibility results over temperature. The attenuation of 0.01 is reached by 11.6 Hz for the entire temperature range of –10 C to –65 C. Amplification gain factor Q at –10 C (Hot) is just over 3 (3.3). It is apparent that as the temperature gets cold, and the fluid viscosity increases, the amplification of the higher frequency local modes (~ 85 Hz, ~ 130 Hz)

decreases as anticipated, with the exception of the tuning spring surge mode (~ 242 Hz) which has no damping mechanism or coupling into damper motion, and therefore should not change damping over temperature.

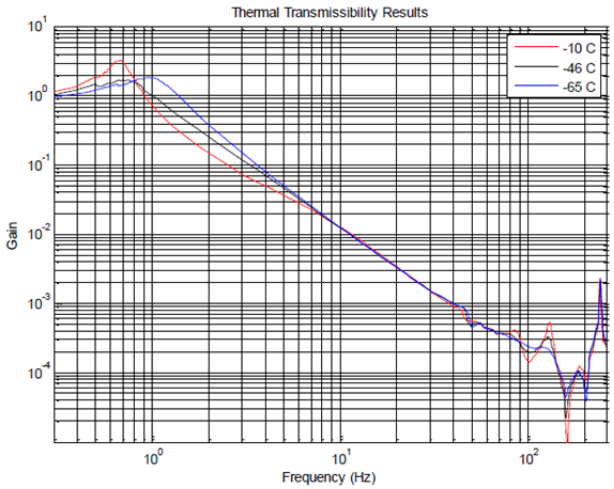

Figure 9. Thermal micro-motion transmissibility test results.

Table 3 summarize SPICA isolator design requirements compliance. As seen, almost all requirement are successfully satisfied as designed. The strut parameters (K_a, K_b and C_a) were obtained from fitting curve plot to a impedance test result. The K_b and C_a parameters were deviated from the design value as estimated. Figure 10 shows 6DOF transmissibility analysis using the fixed-base isolation system model. Design parameters were applied to the model in left figure and test result parameters in right figure. Transmissibility is better than (less than) 0.01 by 15 Hz and $Q < 3$ in all DOF even though the test result parameter is applied. Therefore we concludes that the trial of BBM isolator is a great success while some minor improvement are found:

- C_a compliance is a easily achieved with changing the nominal fluid viscosity used.
- K_b compliance would involve a change to the tuning spring stiffness, but it is believed the 'as-built' higher K_b isolator would meet actual program needs due to the higher available damping it permits.

Table 3. Isolator design requirements compliance.

Specification	Design requirement	BBM result	Test result
K_a	1576.1 – 2626.9 N/m	1714.5 N/m	Compliant
K_b	1926.4 – 2977.2 N/m	3152.3 N/m	Conditionally compliant
C_a	366 N/(m/s) +/– 7.5%	297.7 N/(m/s) @–46C	Conditionally compliant
Stroke	2 mm pull-down + launch load	+/–3.3 mm	Compliant
Temperature range	Operational : –65 C to –10 C Survival : –65 C to +60 C	–65 to +23 C tested	Compliant
Length	<203.2 mm	200.7 mm measured	Compliant
Strut mass	< 2 kg/isolator	0.76 kg	Compliant
Fluid viscosity	< 30 cS	5 cS	Compliant

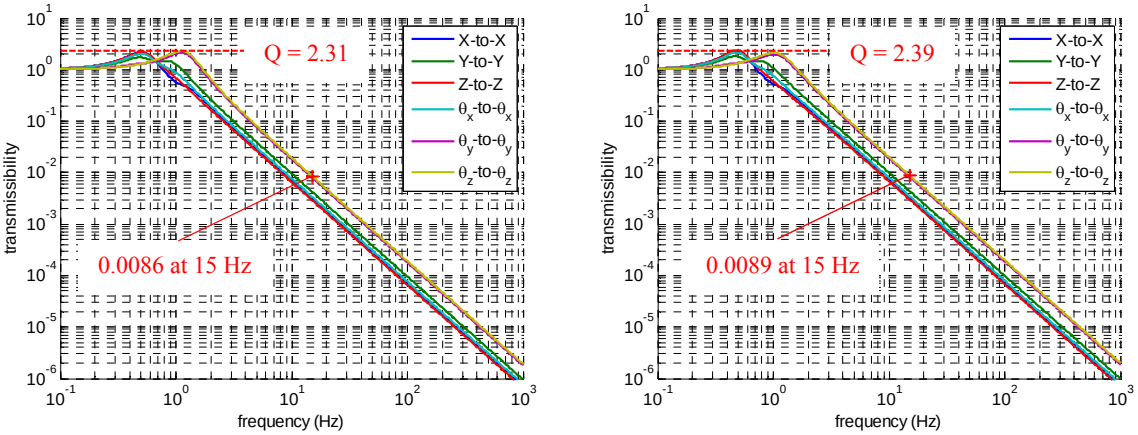

Figure 10. Direct transmissibility (Left: design value, Right: fitting value from test result).

5. TTM DESIGN AND PERFORMANCE TEST

5.1 Requirement and design concept

Table 4 shows the TTM specification. To reduce the development risk and overall cost, both TTM mechanisms of MCS and SCI are required to be designed as exactly same design. The mirror is accurately pointed within 5 mas (3σ) for SCI's stability requirement is 60 mas (0-P). And remarkable specification is 1 mW of ultra-low heat dissipation requirement.

For 0.025 deg of wide mechanical angle (equivalent to 3 arcsec of optical coverage angle), the robustness of the mechanism, and 1 mW of heat dissipation, choosing electromagnetic attraction type such as stepping motor and DC/AC motor could be optimal solution. As candidates of the local sensor for detecting the mirror moving angles, type laserdiode-quadrant detector, eddy current sensor, capacitance sensor are considered for example. However there are difficulties of installed space, weight and heat dissipation while installing the sensor is preferable in terms of good accuracy. Therefore concept of open-loop drive type without any local sensors was proposed and studied. A 2-phase stepping motor technologies which does not rely on the local sensor feedback was applied.

Using the stepping motor technology, wide drive range is achieved by the number of stepping command and driving accuracy can be ensured with micro-stepping resolution. In order to keep dynamic resolution 3 / 0.005 = 600 (coverage angle to control accuracy) and to convert large motor step angle to fine mirror angle, pendulum-like mirror drive mechanism with 1 / 700 of reduction ratio (mirror angle / motor angle) has been manufactured. Figure 11 shows fabricated TTM BBM mechanism. The bottom of annular mechanism converts stepping motor angle to the mirror tilt angle via pendulum-like arms. Dummy load equivalent to the mirror mass property is mounted instead of an actual mirror.

Table 4. Specification of Tip-Tilt Mirror (TTM) for FPIs.

Item	Requirement
Feature	Common design for MCS and SCI
Control accuracy	0.005 arcsec (3σ): converted to optical axis 0.15 arcsec (3σ): converted to mechanical axis
Frequency response	>1 Hz (10 Hz : Goal)
Coverage for acquisition / tracking	>3 arcsec : converted to optical axis >0.025 deg : converted to mechanical axis
Operating temperature	Operational : 4 K to 10 K Survival : 4 K to 300 K
Heat dissipation	<1 mW at 4.5K
Effective size of mirror	50 mm × 75 mm

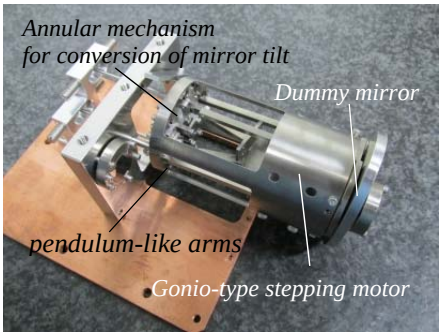

Figure 11. Picture of TTM BBM mechanism for MCS and SCI.

5.2 Cryogenic test result

Produced TTM BBM has been evaluated with a cryogenic chamber (shown in Figure 12) [12]. At first, TTM can be performed to work correctly with 17mAo-p as the drive current in Room Temperature (RT) test. However, in the cryogenic test, 30 mAo-p was necessary for proper operation. Except this fact, the driving performance are well and similar to that in room temperature. Using 4-wire measurement method, the resistance of the drive coil below 10 K and was 5 Ω, which is 1/40 compared to the value in RT. Accordingly, in the cryogenic temperature, the power consumption for driving per 1-axis can be estimated as $5\ \Omega \times (30\ \mathrm{mA_{0-p}}/\sqrt{2})^2 \times 2\ \mathrm{phase} = 4.4\ \mathrm{mW}$.


Figure 12. Cryogenic chamber for TTM mechanism test [12].

The factors to consume more current in the lower temperatures are considered to be increase of the motor detent torque or stiffness change of the reduction mechanism. Since it has been found that a large current for the motor to start to move is required, it is most likely that the motor detent is increased with the result of the gap reduction or the parameters change of the magnetic material at cryogenic temperature.

Table 5 summarizes TTM isolator design requirements compliance. As described above, dissipation power (heat dissipation) is deviated 8.8 times from requirement (for 2-axis drive conversion). Mechanical coverage range is also deviated from the requirement. The factor stems mainly from some difficulties of mechanical tuning sensitivity to the reducing ratio. Static mirror pointing accuracy is measured directly using a theodolite LEICA TM-5100A through the optical window of the chamber. Direct mirror pointing accuracy is confirmed to be within 1.8 arcsec (0.0005 deg) accuracy including reading error while measurement accuracy is insufficient to the requirement 0.15 arcsec (3 σ). For additional verification, the motor 1/10 micro-stepping angle (0.025 deg of resolution requirement) is measured using the same theodolite. The result shows in Fig. 13 left and the micro-stepping accuracy is confirmed. Dynamic property is good up to 1 Hz, while dynamic operation with more frequency tends to need more power consumption.

Table 5. TTM design requirements compliance.

Specification	Requirement	BBM result	Test result
Dissipation power	1 mW per 2-axis @4.5 K	4.4 mW per 1-axis @ 10 K	Non-compliant
Pointing error (mechanical)	0.15 arcsec (3 σ)	< 1.8 arcsec	Conditionally compliant
Frequency response	1 Hz	1 Hz	Compliant
Mechanical coverage range	0.025 deg, P-P	0.016 deg, P-P	Non-compliant
Operational temperature	4 K to 10 K	< 10 K	Compliant
Mirror size	50 mm × 75 mm	50 mm × 75 mm	Compliant
Drive mechanism envelope	50 mm × 50 mm x 100 mm	ϕ 50.1 mm × 104.92 mm	Conditionally Compliant
Weight	600 g	< 420 g	Compliant

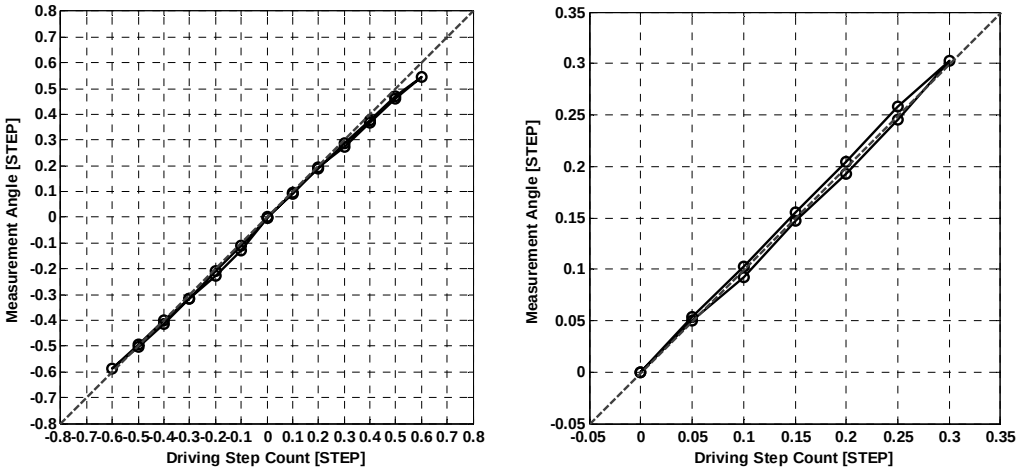

Figure 13. Test results of Motor stepping drive hysteresis (Left: 1/10 step as current design, Right: 1/20 step to attempt).

As conclusion, it was confirmed that TTM BBM functions properly even in the below 10 K environment. TTM concept mechanism which does not require the feedback of the local sensor was demonstrated and static accuracy and dynamic property were confirmed on the condition of the measuring limitation.

However, the requirement of power consumption, and driving range was not achieved. For driving range, there is some difficult adjustment of the reduction mechanism. This issue will be overcome by fleshing out the detail of the manufacturing design. For power consumption, it is possible to satisfy specifications finally by following measures:

- The possible idea is proposed to change the material and design of driving coil to enhance torque scale factor (the ratio of the motor torque to the current). By changing the permalloy C with 3 times permeability than the permalloy B used and by increasing 3 times the cross-sectional area of the motor core design, 1/27 reduction of the power consumption is expected.
- From result of additional experiments, it was found that more fine step up to 1/20 motor step resolution can be designed (shown in Figure 13 right), while currently designed to be 1/10 step resolution. This change contributes to decrease to 1/350 from 1/700 of the reduction ratio. In consequence reducing power consumption might be expected because the motion of the lever mechanism needs half effort.

6. CONCLUSION

In SPICA RMP from 2012 to 2014, activities to be undertaken include consolidation of micro-vibration control design for the satellite, as well as a number of breadboarding activities centered on technologies that are critical to the success of the SPICA mission. This paper presented the RMP activity results on the micro-vibration control design.

- Detailed pointing stability analysis are performed with constructed spacecraft finite element model. In order to achieve pointing jitter allocation in high frequency while maintaining 10-fold margin, it is necessary to circumvent the pedestal resonances from the cryocooler harmonics and to confine the RW operating speed to some extent.
- Isolator BBM for cryocoolers has been fabricated and micro-motion transmissibility test was conducted over the operational temperature range (–65 C to –10 C). Isolator BBM was successfully performed and satisfied the all specifications.
- TTM BBM for SCI and MCS-WFC has been fabricated and evaluated with a cryogenic chamber. It was confirmed that TTM BBM functions properly even in the below 10 K environment. However, the requirement of power consumption and driving coverage were not achieved.

ACKNOWLEDGEMENTS

The authors would like to gratefully acknowledge the following individuals who supported a part of this study: Hiroshi Iida, Koetsu Fujiwara, and Norihiko Mochida (NEC) for the designing of FE model; Brian Workman and Timothy Hindle (Honeywell) for the designing and manufacturing of isolator; Toshihiro Kurii (NEC) for manufacturing and supporting cryogenic test of TTM; Misuzu Haruki (JAXA) for evaluating components disturbance level; Dae-Hee Lee, Woong-Seob Jeong (KASI) and Toshio Matsumoto (ASIAA) for the FPC-G performance study; Gerald Crone (ESA) and Kuo-Chia Liu (NASA) for having technical workshop for SPICA micro-vibration issue.

REFERENCES

[1] Nakagawa, T., Matsuhara;H., and Kawakatsu, Y., "The Next-generation Infrared Space Telescope SPICA", Proc. SPIE 8442 (2012).
[2] Nakagawa, T., Matsuhara, H., Kawakatsu, Y., and Roelfsema, P., "The next-generation infrared astronomy mission SPICA under the new framework," Proc. SPIE 9143 (2014).
[3] Matsuhara, H., Nakagawa, T., Kawakatsu, Y., Murakami, H., Kawada, M., Sugita, H., and et., al., "Cooled Scientific Instrument Assembly onboard SPICA", Proc. SPIE 8442 (2012).
[4] Mitani, S., Iwata, T., Fujiwara, K., Sakai, S., Enya, K., Kotani, T., and et., al., "Precision Pointing Control for SPICA : Requirements and Feasibility Study", Proc. SPIE 7731 (2010).
[5] Bruijne, J., "Status of the GAIA Spacecraft Development", Societe Francaise d'Astronomie et d'Astrophysique (2009).
[6] ESA Website, "#12: GAIA Flight Model Testing Completed", http://sci.esa.int/gaia/51955-journal-12-flight-model-testing-completed/ (2013).
[7] Mizutani, T., Yamawaki, T., Komatsu, K., and et., al., "Preliminary Structural Design and Key Technology Demonstration of Cryogenic Assembly in the Next-generation Infrared Space Telescope SPICA", Proc. SPIE 9143 (2014).
[8] Liu, K., Maghami P., and Blaurock, C., "Reaction Wheel Disturbance Modeling, Jitter Analysis, and Validation Tests for Solar Dynamics Observatory", AIAA Guidance, Navigation and Control Conference and Exhibit, Honolulu, Hawaii (2008).
[9] Mosier, G., Femiano, M., Ha, K., Bely, P., Burg, R., Redding, D., and et., al., "Fine Pointing Control for a Next Generation Space Telescope", SPIE 3356 (1998).
[10] Davis, P., Cunningham, D., and Harrell, J., "Advanced 1.5 Hz Passive Viscous Isolation System", Presented at the 35th AIAA SDM Conference Hilton Head, South Carolina (1994).
[11] Davis, T., Davis, P., Sullivian, J., Hoffman, T., Das, A., "High Performance Passive Viscous Isolator Element for Active/Passive (Hybrid) Isolation", SPIE 2720 (1996).
[12] Enya, K., Haze, K., Kataza, H., Sarugaku, Y., Wada, T., Kotani, T., and et., al., "Prototype-testbed for Infrared Optics and Coronagraphs (PINOCO)", Proc. SPIE 8442 (2012).